Advanced Analysis and Seismic Design of Concrete-Filled Steel Tube Structures

Mark D. Denavit[1]; Jerome F. Hajjar[2]; Roberto T. Leon[3]; and Tiziano Perea[4]

[1]Design Engineer, Stanley D. Lindsey and Associates, Ltd., Atlanta, GA 30339.
[2]CDM Smith Professor and Chair, Department of Civil and Environmental Engineering, Northeastern University, Boston, MA 02115.
[3]Professor, Department of Civil and Environmental Engineering, Virginia Tech, Blacksburg, VA 24061.
[4]Professor, Departamento de Materiales, Universidad Autónoma Metropolitana, Mexico City, Mexico.

Abstract

This paper will focus on aspects of the advanced analysis and underlying behavior of composite structures with concrete-filled steel tube (CFT) columns. Through a detailed examination of the results of a suite of full-scale slender CFT beam-column tests, insight into the cyclic behavior of such members is gained, specifically pertaining to local buckling of the steel tube and the plastic hinge length. Modeling techniques, which capture these behaviors, are introduced and incorporated into a general purpose distributed plasticity fiber based beam element formulation. The model is found to be capable of capturing the observed behavior and producing accurate results.

INTRODUCTION

Advanced analysis models that can faithfully capture the salient features of the nonlinear response of a structure are crucial to the assessment of seismic behavior and the development of seismic design recommendations. For example, nonlinear analysis is central to the FEMA P695 procedure for quantifying seismic performance factors (FEMA 2009). Fiber based beam finite elements are well suited to concrete-filled steel tube (CFT) frame structures. Such models provide accurate results as well as practicality in both model building and computational time. Beam elements accurately capture both material and geometric nonlinearity. Fiber cross sections with appropriate uniaxial stress strain models naturally span the range from concrete dominant to steel dominant members. The calibration and validation of analysis models draws on both theory and experimental results to ensure that the underlying behavior has been represented in the most appropriate manner.

In this paper, a set of detailed experiments on full-scale slender CFT beam-columns and an analysis model specifically calibrated for CFT members are introduced. Then two aspects of behavior are examined in detail with respect to both the experimental results and the nonlinear analysis model. Local buckling of the steel tube is examined first, followed by the plastic hinge length.

FULL-SCALE SLENDER BEAM-COLUMN TESTS

A series of experiments have been performed on a set of full-scale slender CFT beam-columns. The specimens in the experimental program were selected to be both relatively slender in length and in steel tube width-to-thickness ratio. In total, eighteen specimens were tested with variations in steel tube shape and size, length, and concrete strength (Table 1).

Table 1. Experimental Text Matrix

Specimen	*D* or *H* (mm)	*B* (mm)	*t* (mm)	f'_c (MPa)	F_y (MPa)	*L* (mm)	*R* (---)	$\varepsilon_{lb}/\varepsilon_y$ (---)
1-C5-18-5	141	---	3.15	37.9	383	5,499	0.086	14.19
2-C12-18-5	324	---	5.92	38.6	337	5,499	0.092	n/a
3-C20-18-5	508	---	5.92	40.0	328	5,525	0.141	5.09
4-Rw-18-5	508	305	7.39	40.7	365	5,537	0.0030	1.64
5-Rs-18-5	508	305	7.39	40.7	365	5,537	0.0065	3.57
6-C12-18-12	324	---	5.92	91.0	337	5,499	0.092	n/a
7-C20-18-12	508	---	5.92	91.0	328	5,534	0.141	4.51
8-Rw-18-12	508	305	7.39	91.7	365	5,553	0.0025	1.37
9-Rs-18-12	508	305	7.39	91.7	365	5,553	0.0058	3.16
10-C12-26-5	324	---	5.92	54.5	335	7,950	0.092	10.74
11-C20-26-5	508	---	5.92	55.8	305	7,995	0.131	6.61
12-Rw-26-5	508	305	7.39	56.5	406	7,957	0.0026	1.28
13-Rs-26-5	508	305	7.39	57.2	383	7,969	0.0075	3.92
14-C12-26-12	324	---	5.92	80.0	383	7,963	0.105	8.10
15-C20-26-12	508	---	5.92	80.0	293	7,976	0.126	6.35
16-Rw-26-12	508	305	7.39	80.7	381	7,957	0.0023	1.21
17-Rs-26-12	508	305	7.39	80.7	380	7,963	0.0062	3.26
18-C5-26-12	141	---	3.15	80.7	383	7,941	0.086	n/a

Note: In this table, D is the diameter of the circular section, B and H are the width and depth of the rectangular section respectively, t is the thickness of the steel tube, F_y is the measured yield stress of the steel tube, f'_c is the concrete strength at the testing day, L is the measured length, R is a slenderness parameter (Figure 3), and $\varepsilon_{lb}/\varepsilon_y$ is the measured strain at initiation of local buckling normalized by the yielding strain.

The tests were conducted at the Multi-Axial Sub-Assemblage Testing (MAST) facility at the University of Minnesota. The MAST system (Figure 1) consists of a stiff steel crosshead connected to 4 vertical actuators and 2 actuators in both horizontal directions, allowing 6 DOF control of the crosshead. Thick plates were welded to the ends of the specimens. The bottom plate rigidly connected the specimen to the strong floor and the top plate rigidly connected the specimen to the crosshead. Through control of crosshead different end conditions could be simulated, most often a fixed-free (K=2) condition was enforced.

The specimens were subjected to a variety of successive load cases. The first load case subjected the specimens to concentric axial load. In this load case, most specimens were held in a fixed-free (K=2) configuration [specimens 1-C5-18-5 and 18-C5-26-12 were held in a fixed-fixed (K=1) configuration]. Specifically, lateral forces and bending moments at the crosshead were force controlled to zero, while the specimen was loaded axially in displacement control until the critical load was reached. The twist DOF was held in displacement control to zero. Detailed results from this first load case are reported by Perea *et al*. (2013).

The second load case subjected the specimens to combined axial compression and uniaxial bending. This was achieved with vertical force control at a specified load and

displacement control of the lateral DOFs. Again, most specimens were held in a fixed-free (K=2) configuration with bending moments at the crosshead were force controlled to zero [specimens 1-C5-18-5 and 18-C5-26-12 were held in a fixed-fixed (K=1) configuration]. The third load case maintained the same control as the second load case, but subjected the specimen to combined axial compression and biaxial bending. Detailed results from the second and third load cases are reported by Perea *et al*. (2014).

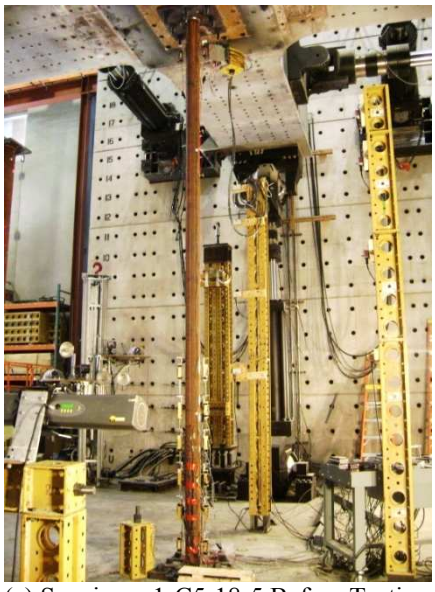

(a) Specimen 1-C5-18-5 Before Testing

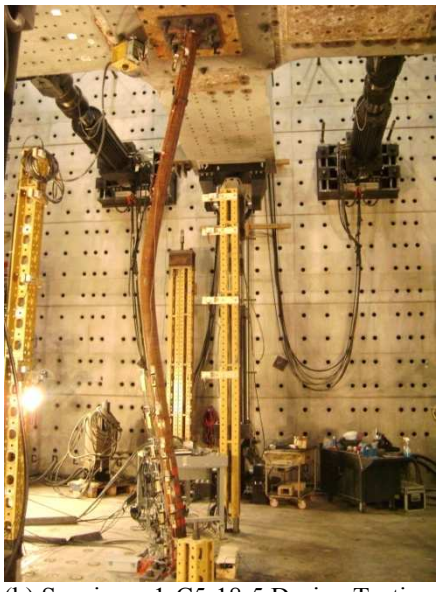

(b) Specimen 1-C5-18-5 During Testing

Figure 1. Specimen 1-C5-18-5 in the MAST Facility

Additional latter load cases were conducted, subjecting the specimens to torsion or alternate end conditions. Full details of the test program including these load cases and discussions on wet concrete effects are presented elsewhere (Perea 2010; Perea et al. 2013, 2014).

MIXED BEAM FINITE ELEMENT FORMULATION

Frame analyses using distributed plasticity beam elements strike a favorable balance of computational efficiency and accuracy. Additionally, mixed formulations (defined here as treating both element displacements and stress resultants as primary state variables) allow for accurate modeling of both geometric and material nonlinearities. Tort and Hajjar (2010b) developed a three-dimensional mixed beam element for the analysis of composite frames that include rectangular concrete-filled steel tube members. This finite element was adapted and further validated against an additional sets of experimental tests on circular concrete-filled steel tube members (Denavit and Hajjar 2012).

The formulation relies on accurate constitutive relations to achieve accurate results. Numerous uniaxial constitutive relations have been proposed for composite members (e.g., Sakino et al. 2004). Typically, the relations are unique to the member shape (circular, rectangular, etc.) because of differences in behavior, namely different confinement of the concrete and different susceptibility to local buckling (which is

often modeled as a material response). Different models use different assumptions and methods of calibration, but they generally strive to mimic the response of short concentrically loaded columns.

As part of the mixed beam formulation, a family of accurate uniaxial cyclic material models have been developed and reported by Tort and Hajjar (2010a) for RCFTs and Denavit and Hajjar (2012) for CCFTs. The constitutive relation for the concrete core is adapted from the rule-based model of Chang and Mander (1994). The tensile branch and the cyclic rules were used without changes. However, the compressive branch was altered to reflect the state of confinement existing in the composite members. The steel model is based on the bounding-surface plasticity model of Shen et al. (1995). Several modifications were made to model the behavior of the cold formed steel tubes in CFT sections, including modifications to allow for the modeling of local buckling as will be discussed in the following section.

To validate the models, hundreds of comparative analyses were performed (Denavit and Hajjar 2012, 2014; Tort and Hajjar 2010a). Sets of experimental data covering a wide variety of material properties, geometric properties, and loading configurations assembled. The slender beam-column tests described in the previous section were included in the validation study.

LOCAL BUCKLING OF THE STEEL TUBE

Under compressive stress, the steel tube of a CFT member is susceptible to local buckling. Due to the presence of the concrete core, the steel tube only has the ability to buckle outward. In a detailed analysis with continuum or shell elements, local buckling behavior can be captured explicitly. In frame analyses with beam elements, this behavior can only be accounted for implicitly in the material constitutive relation. As mentioned in the previous section, the stress-strain constitutive model for steel adopted in this work is based on a bounding surface plasticity model. To account for local buckling the model is modified to consist of three regions in compression (Figure 2). The first region is the unmodified Shen et al. (1995) model, beginning with elastic behavior then continuing into plasticity. The second region is commences after the initiation of local buckling, which is assumed to be occur when the compressive strain reaches a prescribed value, ε_{lb}. In this region the response from the plasticity model is overridden by linear strength degradation with a prescribed modulus, K_{slb}. The third region is a constant ultimate residual stress, F_{ulb}. Further rules and modifications are necessary to properly model the local buckling response under cyclic loading (Denavit and Hajjar 2014).

In the steel constitutive relation, the strain at which local buckling initiates, ε_{lb}, is taken as a function of a measure of tube slenderness (Figure 3). The function was calibrated to experimental data found in the literature where initiation of local buckling was clearly identifiable or was noted by the author in the original reporting (Denavit and Hajjar 2012; Tort and Hajjar 2010a). This data is denoted in Figure 3 as the “calibration data” and is shown with grey markers. Comparable experimental data from the slender beam-column tests discussed in this paper (but not used in the

calibration of the steel constitutive relation) is denoted in Figure 3 as the "current data" and is shown with red markers.

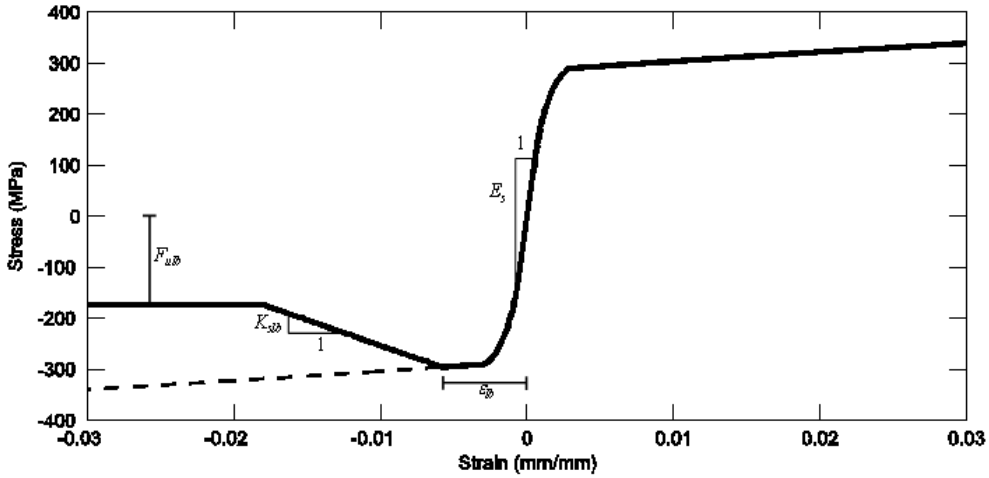

Figure 2. Steel Stress-Strain Relationship including Local Buckling

Several means were employed in the determination of the first occurrence of local buckling in the slender beam-column tests. The most basic means of detecting local buckling was through visual inspection, though, this method was limited. Despite the numerous still and video cameras with different views and angles of the specimens employed during the tests, local buckling was often not visible until the buckles were severe. Safety concerns and time constraints limited the frequency that close observations, where the initiation of local buckling could be more reliability identified, could be made.

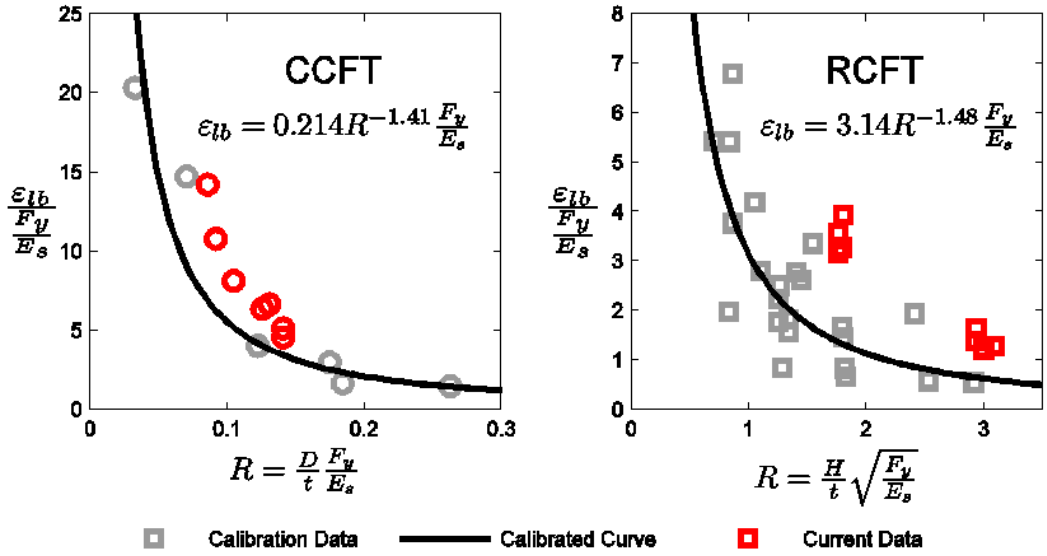

Figure 3. Strain at Local Buckling Data

Beyond the visual observations, two sets of instrumentation aided in identifying local buckling. A Krypton coordinate measurement machine was utilized to measure the three-dimensional location of LEDs placed on the specimen (visible in Figure 4a). Using this data, significant out-of-plane motion of one LED relative to the others

would indicate local buckling. Additionally, strain gages were placed longitudinally in three locations around the perimeter of the tubes and intermediately along the height of the specimens. Sharp increases in the strain would also indicate local buckling. The strain gages were also used to determine the compressive strain in the specimen at which the local buckling first occurred.

The experimentally obtained strains at initiation of local buckling are presented in Table 1 along with the computed tube slenderness parameter, R. The data is normalized with respect to the yield strain $\varepsilon_y = F_y/E_s$ and not given for the three specimens for which local buckling was not observed. The data from the slender beam-column tests is also presented in Figure 3 as "current data" with red markers along with the empirical expression used in the constitutive relations and the set of prior experimental data used in the calibration of the empirical expression (denoted as "calibration data" with grey markers). The strain at initial local buckling from the slender beam-column tests is consistently higher than predicted by the empirical expression, indicating that local buckling occurred later than predicted in the loading. The reason for the discrepancy could be due to different methods of identifying the initiation of local buckling, the relatively lower axial loads and higher bending moments in the slender beam-column tests as compared to the calibration data, or simply random variation since the calibration data is rather sparse and variable.

(a) Specimen 10-C12-26-5 (b) Specimen 8-Rw-18-12

Figure 4. Local Buckling Deformation at the Conclusion of Testing

The ability to model local buckling is important as it can have a strong effect on the results, especially for members under severe cyclic loading. In Figure 5, a comparison of experimental and computational results for one of the rectangular slender beam-column specimens is presented. Two sets of computational results are shown: one which includes modeling of local buckling and one in which the local buckling aspects of the constitutive relation were inactive. In the first load case, the analysis without local buckling more accurately matches the experimental results. The peak load in the analysis with local buckling is lower, likely due to premature local buckling as discussed previously. In the second load cases (LC2a with axial compression = 2,669 kN and LC2b with axial compression = 1,334 kN) there is little

difference between the two sets of analysis results and both match the experimental results well. The results start to significantly diverge in the third load case (LC3a with axial compression = 3,559 kN). In this load case, under higher axial compression and biaxial loading, local buckling causes severe strength degradation. The state of the specimen at the conclusion of testing is shown in Figure 4b. The analysis with local buckling captures this behavior matching the results with good accuracy. The analysis without local buckling does not capture the strength degradation and yields a poor comparison.

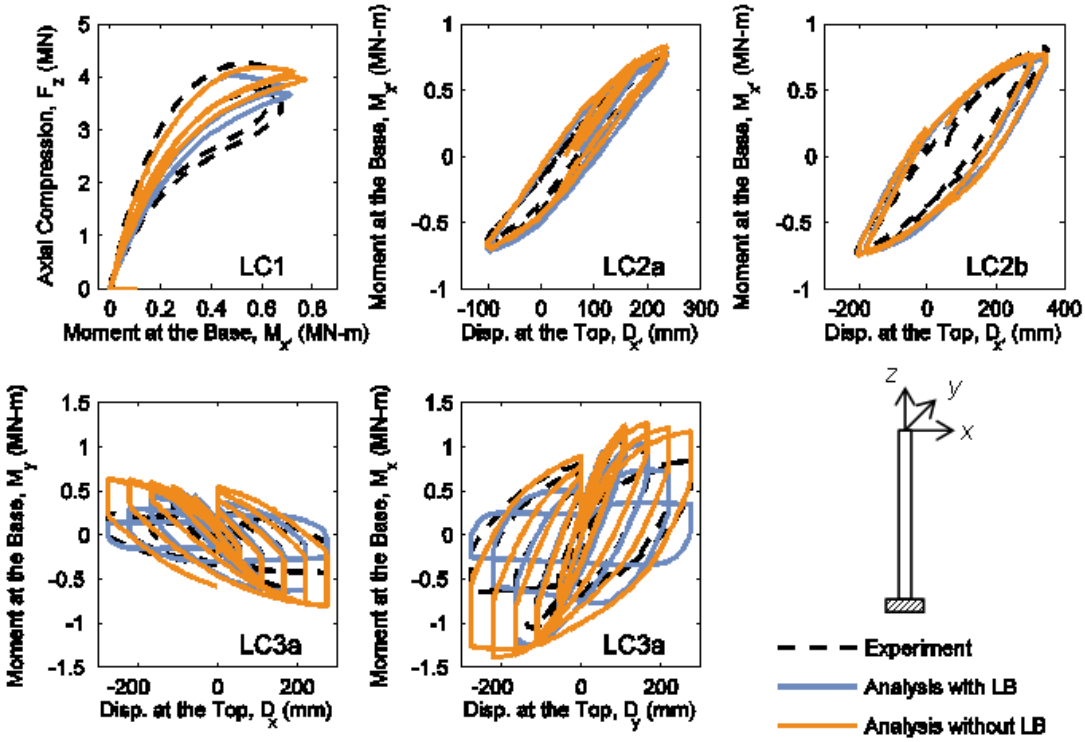

Figure 5. Comparison of Validation Results – Specimen 8-Rw-18-12

PLASTIC HINGE LENGTH

Regions of beams and columns that experience large inelastic curvatures when subjected to severe loading are designated plastic hinges. The inelasticity generally occurs in certain critical locations (e.g., the member ends for reverse curvature bending) and over a finite length, which is termed the plastic hinge length. The plastic hinge length has important implications for finite element analyses (Attalla et al. 1994) as well as for design. Distributed plasticity models, such as the one adopted in this work, track inelasticity throughout the entire length of the element. For strain-hardening sections, the plastic hinge length develops naturally and can be observed in analyses. However, for strain-softening sections, to maintain equilibrium, typically only one section in the element will follow the softening path, while the others simply unload elastically. The portion of the element over which the softening section is applicable is dependent on the numerical integration weight assigned to the section which depends on the number of sections. This causes a loss of objectivity and

computed results vary significantly based on the selected mesh density. This phenomenon is known as localization.

Localization has been studied in the context of force based beam elements (Coleman and Spacone 2001; Scott and Fenves 2006; Scott and Hamutcuoglu 2008). Two general solutions have been proposed, the first is the alteration of the softening slope of the constitutive relations, and the second is to ensure that the numerical integration is performed such that the softening effects are distributed along the appropriate length of the member, i.e., the integration weight assigned to the section which softens represents the physical plastic hinge length.

Scott and Hamutcuoglu (2008) present a specialized numerical integration scheme based on Lobatto quadrature but with the ability to prescribe the integration weights at the element ends. This approach, when implemented in the mixed beam element, performs very well for many cases, eliminating the mesh dependency associated with localization. However, the special numerical integration scheme can cause difficulty in obtaining convergent results. Alternatively, a simple approximate method of handling localization can be used whereby the mesh density (i.e., number of elements per member and number of integration points per element) is selected such that the integration weight implied by Lobatto quadrature of the critical integration point (section highest moment) is approximately equal to the physical plastic hinge length. This approach, however, has limitations. Aspects of the physical behavior such as the moment gradient must be known a priori and often a mesh cannot be selected such that the region of expected inelasticity is represented by a single integration point or even a single element. Nonetheless, with an estimation of the physical plastic hinge length and careful selection of the mesh density, accurate results can be obtained for a vast majority of practical cases.

Instrumentation of the slender beam-column specimens, in particular the sets of strain gages placed longitudinally along the height of the column, allow for measurement of the curvature distribution from which the plastic hinge length can be estimated. The distribution of curvature within eight of the circular specimens is shown in Figure 6. These curvature distributions were obtained at the peak lateral displacement during one of the load cases. The selected load case was the last case in the load history that provided high curvatures and consistent strain gauge data. The strain data in some of the latter cases was not be reliable (mainly near the member bottom) due to saturated measurements or detached strain gauges as a consequence of excessive local buckling.

The curvature distributions shown in Figure 6 follow the expected shape. The loading for these cases is that of a cantilever column with vertical and horizontal loads (Figure 7a), with an approximately triangular moment distribution (neglecting P-Δ effects). Correspondingly, in the upper portion of the specimens, where the cross sections remained mostly elastic, the curvature distribution was approximately linear. Higher curvatures are noted in the lower portion of the specimen where the bending moment was the highest and the cross sections exhibited plastic deformations. From this experimental data, the plastic hinge length is roughly 20-30% of the column length.

The experimental data provides a good estimate of the plastic hinge length for the particular specimens investigated. However, the estimate is intended to be used to inform the finite element mesh density and a general analysis procedure is desired. Therefore, additional estimates are necessary for a wide range of cases. Additional estimates of the plastic hinge length can be made analytically through a nonlinear cross section analysis using the same fiber discretization used in the mixed beam finite elements. Examining a prototypical cantilever beam-column (Figure 7a), the plastic hinge length, L_p, may be approximated by Equation 1 (L_p normalized by the length from the point of maximum moment to the point of zero moment, L_i).

$$\frac{L_p}{L_i} = 1 - \frac{M_y}{M_u} \tag{1}$$

To obtain the plastic hinge length using this expression, two values are required: the yield moment, M_y, and the ultimate moment, M_u. The ultimate moment has a relatively straightforward definition and can be obtained by identifying the peak moment from the moment-curvature response (Figure 7b). The yield moment, however, does not have an obvious definition, owing to the gradual transition to plasticity seen in the moment-curvature response. Prior studies have used different definitions to identify the yield moment. Elghazouli and Elnashai (1993) performed this type of study on partially encased composite columns and identified the yield moment as the moment at which the yield strain was reached in both the tensile and compressive extreme fibers. Bae and Bayrak (2008) performed this type of study on reinforced concrete columns and identified the yield moment as the moment at which the yield strain was reached in the compressive steel reinforcement.

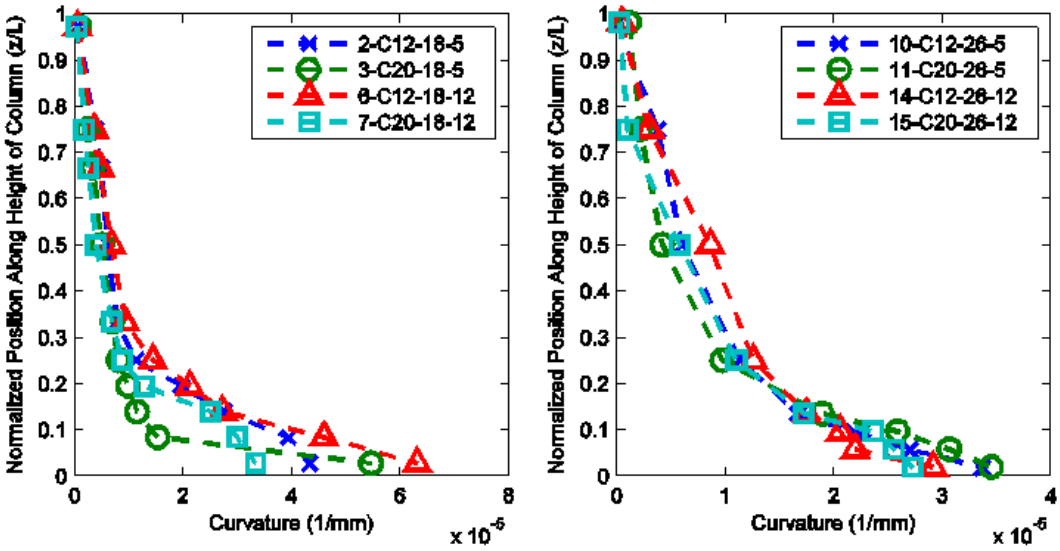

Figure 6. Experimental Curvature at Peak Lateral Displacement

In this study, the yield moment is defined directly from the moment-curvature response using an offset methodology analogous to that used to define the offset yield stress from tensile coupon tests that do not exhibit a clear yield point. The yield moment is defined as the moment that corresponds to the point of intersection of the moment-curvature response and a line parallel to the initially linear portion of the

response. The slope of the parallel line is taken as the secant stiffness from zero moment to 45% of the ultimate moment. The offset is the distance between the origin of the moment-curvature response and the point of intersection of the parallel line and the zero moment axis. The offset is expressed in terms of curvature and is taken as $0.001/D$, where D is the overall section depth. This value was selected based on inspection of results from typical composite cross sections as the point at which the initiation of significant plastic deformations typically occurred.

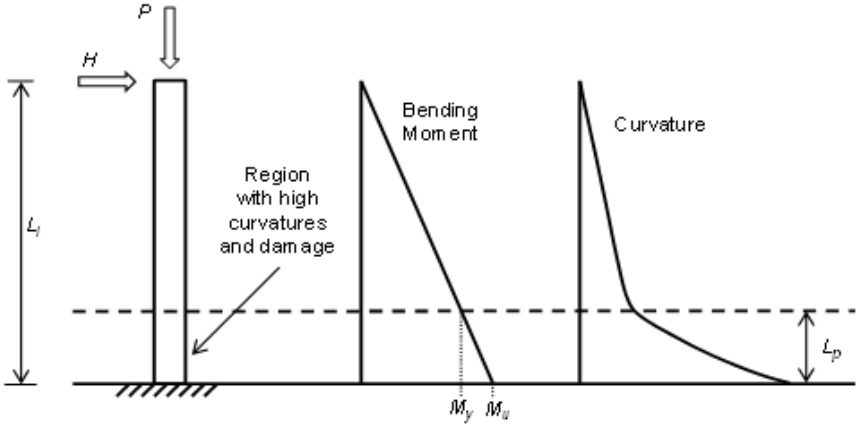

(a) Prototypical Beam-Column

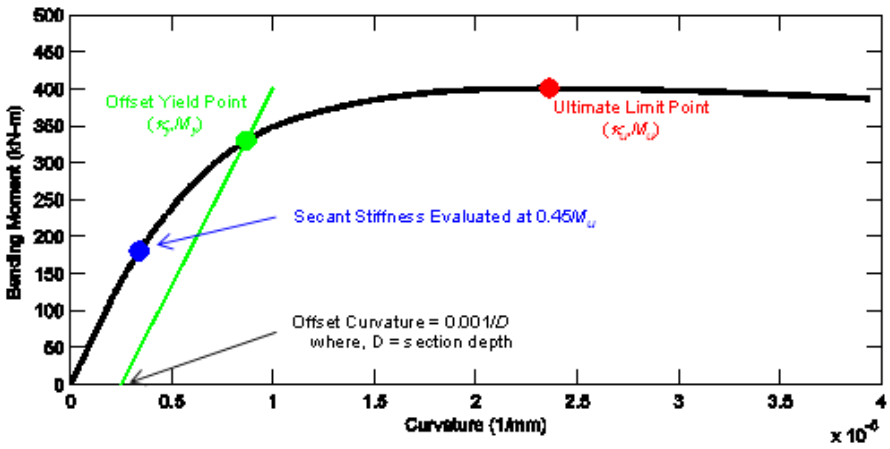

(b) Moment Curvature Results

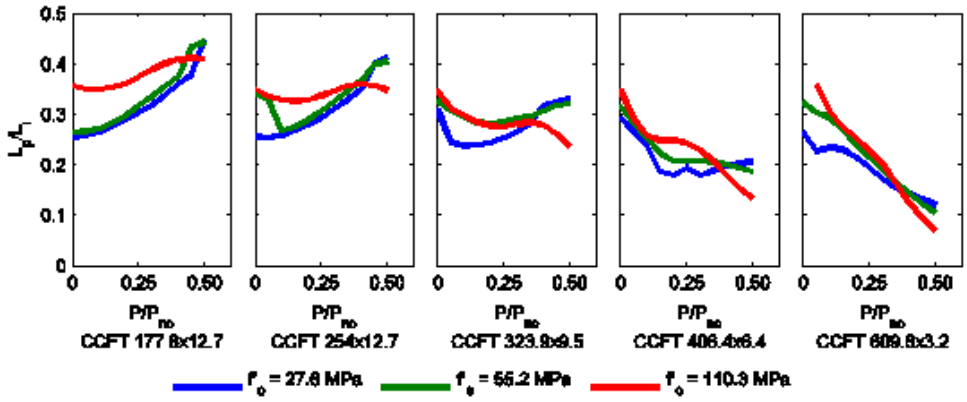

(c) Results for CCFT Sections

Figure 7. Schematic of Plastic Hinge Length Methodology and Results

The plastic hinge length obtained from this methodology will vary with the given cross section as well as the applied axial load. Thus, a parametric study was performed to document the variation of the plastic hinge length with material, geometric, and loading properties. Five circular HSS sections (HSS177.8×12.7, HSS254×12.7, HSS323.9×9.5, HSS406.4×6.4, and HSS609.6×3.2) were selected to span the range of permissible steel ratios and three concrete strengths (f'_c = 27.6, 55.2, and 110.3 MPa) were selected for a total of 15 circular CFT cross sections. Steel yield strength was taken as the typical nominal value (F_y = 290 MPa). A moment-curvature analysis was performed for each cross section and for compressive axial loads ranging from zero to 50% of the cross section capacity, P_{no}, identifying M_y and M_u for each analyses to determine L_p/L_i. Results are shown in Figure 7c. The results show that the plastic hinge length varies with steel ratio, concrete strength and axial load. The greatest variations occur with axial load for the more concrete dominant sections. The analysis results match generally well with the experimental results which indicated a value of L_p/L_i between 0.2 and 0.3.

CONCLUSIONS

Two aspects of the behavior of concrete filled steel tube beam columns were discussed. The aspects were highlighted in the context of both a set of experimental results and a nonlinear analysis formulation. Local buckling of the steel tube was identified as a cause of significant strength degradation and a challenging but crucial phenomenon to model. The plastic hinge length was identified as of key importance in mitigating the deleterious effects of localization. Estimates of the plastic hinge length, which may be used when selecting a finite element mesh, were made using both the experimental data and analysis results.

ACKNOWLEDGMENTS

This material is based upon work as part of a NEESR project supported by the National Science Foundation under Grant No. CMMI-0619047, the American Institute of Steel Construction, the Georgia Institute of Technology, and the University of Illinois at Urbana-Champaign. Any opinions, findings, and conclusions expressed in this material are those of the authors and do not necessarily reflect the views of the National Science Foundation or other sponsors.

REFERENCES

Attalla, M. R., Deierlein, G. G., and McGuire, W. (1994). “Spread of Plasticity: Quasi-Plastic-Hinge Approach.” *Journal of Structural Engineering*, ASCE, 120(8), 2451–2473.

Bae, S., and Bayrak, O. (2008). “Plastic Hinge Length of Reinforced Concrete Columns.” *ACI Structural Journal*, 105(3), 290–300.

Chang, G. A., and Mander, J. B. (1994). *Seismic Energy Based Fatigue Damage Analysis of Bridge Columns: Part I - Evaluation of Seismic Capacity*. National Center for Earthquake Engineering Research, Department of Civil Engineering, State University of New York at Buffalo, Buffalo, New York.

Coleman, J., and Spacone, E. (2001). "Localization Issues in Force-Based Frame Elements." *Journal of Structural Engineering*, ASCE, 127(11), 1257–1265.

Denavit, M. D., and Hajjar, J. F. (2012). "Nonlinear Seismic Analysis of Circular Concrete-Filled Steel Tube Members and Frames." *Journal of Structural Engineering*, ASCE, 138(9), 1089–1098.

Denavit, M. D., and Hajjar, J. F. (2014). *Characterization of Behavior of Steel-Concrete Composite Members and Frames with Applications for Design*. Newmark Structural Laboratory Report Series, Newmark Structural Laboratory Report NSEL-034, University of Illinois at Urbana-Champaign, Urbana, Illinois.

Elghazouli, A. Y., and Elnashai, A. S. (1993). "Performance of Composite Steel/Concrete Members under Earthquake Loading. Part II: Parametric Studies and Design Considerations." *Earthquake Engineering & Structural Dynamics*, 22(4), 347–368.

FEMA. (2009). *Quantification of Building Seismic Performance Factors*. FEMA P695, Federal Emergency Management Agency, Washington, D.C.

Perea, T. (2010). "Analytical and Experimental Study on Slender Concrete-Filled Steel Tube Columns and Beam-Columns." Ph.D. Dissertation, School of Civil and Environmental Engineering, Georgia Institute of Technology, Atlanta, Georgia.

Perea, T., Leon, R. T., Hajjar, J. F., and Denavit, M. D. (2013). "Full-Scale Tests of Slender Concrete-Filled Tubes: Axial Behavior." *Journal of Structural Engineering*, ASCE, 139(7), 1249–1262.

Perea, T., Leon, R. T., Hajjar, J. F., and Denavit, M. D. (2014). "Full-Scale Tests of Slender Concrete-Filled Tubes: Interaction Behavior." *Journal of Structural Engineering*, ASCE, 140(9), 04014054.

Sakino, K., Nakahara, H., Morino, S., and Nishiyama, I. (2004). "Behavior of Centrally Loaded Concrete-Filled Steel-Tube Short Columns." *Journal of Structural Engineering*, ASCE, 130(2), 180–188.

Scott, M. H., and Fenves, G. L. (2006). "Plastic Hinge Integration Methods for Force-Based Beam--Column Elements." *Journal of Structural Engineering*, ASCE, 132(2), 244–252.

Scott, M. H., and Hamutcuoglu, O. M. (2008). "Numerically Consistent Regularization of Force-Based Frame Elements." *International Journal for Numerical Methods in Engineering*, 76(10), 1612–1631.

Shen, C., Mamaghani, I. H. P., Mizuno, E., and Usami, T. (1995). "Cyclic Behavior of Structural Steels. II: Theory." *Journal of Engineering Mechanics*, ASCE, 121(11), 1165–1172.

Tort, C., and Hajjar, J. F. (2010a). "Mixed Finite-Element Modeling of Rectangular Concrete-Filled Steel Tube Members and Frames under Static and Dynamic Loads." *Journal of Structural Engineering*, ASCE, 136(6), 654–664.

Tort, C., and Hajjar, J. F. (2010b). "Mixed Finite Element for Three-Dimensional Nonlinear Dynamic Analysis of Rectangular Concrete-Filled Steel Tube Beam-Columns." *Journal of Engineering Mechanics*, ASCE, 136(11), 1329–1339.